REVIEW

Carbon-Based Field-Effect Transistors for Nanoelectronics

By *Marko Burghard,* Hagen Klauk,* and *Klaus Kern*

In this review, the suitability of the major types of carbon nanostructures as conducting channels of field-effect transistors (FETs) is compared on the basis of the dimensionality and size of their π-conjugated system. For each of these materials, recent progress in its synthesis, electrical and structural characterization, as well as its implementation into various gate configurations is surveyed, with emphasis laid onto nanoscale aspects of the FET design and the attainable device performance. Finally, promising future research directions, such as the integration of different carbon nanostructures into novel device architectures, are outlined.

1. Introduction

Carbon is an outstanding element. The isolated carbon atom has a ($1s^2 2s^2 2p^2$) configuration with filled 1s and 2s states and two electrons in the 2p state. Through sp^2 hybridization of the atomic orbitals, two neighboring atoms can bond strongly via both σ- and π-states, with the latter involving the p_z orbitals that are oriented perpendicular to the intersection line between the atoms. Due to the high π-bonding energy, graphite is energetically slightly more stable than sp^3-bonded diamond-like structures under ambient pressure and temperature. Although its neighbors to the right and left in the periodic table (boron and nitrogen) can also form strong π bonds, only carbon occupies the favored position of having exactly four electrons and requiring exactly four bonds to attain a closed shell. Indeed, the ability of carbon to form a wide variety of anisotropic and stable 2D structures is in contrast to clusters of nearly all other elements, which are essentially always 3D.

The fundamental 2D carbon structure is graphene, a honeycomb atomic layer (Fig. 1A) representing the basic structural constituent of graphite. Graphene can be conceptually viewed as an indefinitely extended, 2D aromatic macromolecule. Capping off the edges of very small graphene sheets by hydrogen atoms yields stable π-conjugated molecules such as pentacene,[1] hexabenzocoronene,[2] or picene[3] (Fig. 1B). Further to this, a rich family of structures can be formed by distorting the graphene sheet in the third dimension. Graphene, being a single atom layer, can be bent without appreciably changing the in-plane bond lengths, rendering the energy cost for the distortion relatively small. In order to eliminate dangling bonds, graphene must be wrapped around itself to form a closed structure without edges. As one possibility, the roll-up of graphene results in carbon nanotubes (Fig. 1C), whose ends may be closed by appropriate caps. Another option involves bending the graphene sheet in two dimensions, which yields fullerenes (such as C_{60}, in Fig. 1D). Similar to the nanotube caps, this folding into a closed cage requires the presence of pentagons in addition to hexagons.

The electronic-band structure of graphene combines semiconducting and metallic characteristics, as it can be conceived both as a metal with vanishing Fermi surface and as a semiconductor with a vanishing band gap. This peculiar property stems from graphene's unit cell, comprised of two carbon atoms, which renders the π- and π*-bands indistinguishable at the Fermi energy, such that they remain equal in energy and the two

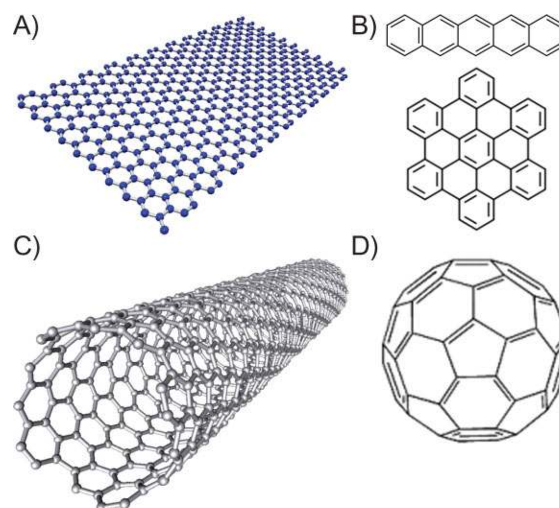

Figure 1. Chemical structures of A) a graphene sheet with its 2D delocalized electron system, B) pentacene (top) and hexabenzocoronene (bottom) as two representative π-conjugated molecules that can be conceived as small graphene sheets with hydrogen-saturated edges, C) a chiral single-wall carbon nanotube with a quasi-1D electron system, and D) the C_{60} fullerene representing a 0D electron system.

[*] Dr. M. Burghard, Dr. H. Klauk, Prof. K. Kern
Max-Planck-Insitut fuer Festkoerperforschung
Heisenbergstrasse 1, 70569 Stuttgart (Germany)
E-mail: m.burghard@fkf.mpg.de
Prof. K. Kern
Institut de Physique de la Matière Condensée
Ecole Polytechnique Fédérale de Lausanne
1015 Lausanne (Switzerland)

DOI: 10.1002/adma.200803582

© 2009 WILEY-VCH Verlag GmbH & Co. KGaA, Weinheim

bands touch each other at the K-point in the Brillouin zone (Fig. 2A). Moreover, the close carbon–carbon distance in graphene leads to a pronounced interatomic overlap that spreads these bands out over a wide energy range, resulting in a rather large Fermi velocity of the electrons ($v_F \approx 10^6$ m s^{-1}). As a consequence of the linear dispersion up to ± 1 eV around the Fermi level, the electrons and holes in graphene behave as if they have no mass, and their electronic density of states (DOS) depends linearly on energy. The 1D band structure of a carbon nanotube can be derived by restricting the 2D energy dispersion of graphene to those wave vectors that remain allowed by quantization along the tube circumference (Fig. 2B). If the corresponding slices pass through graphene's *K*-point, the nanotube is metallic, and otherwise semiconducting. In the simple tight-binding model, the band gap E_g of a semiconducting tube is given by

$$E_g = 4\hbar v_F / 3 d_{CNT} = \gamma (2 R_{C-C} / d_{CNT})$$

where γ is the hopping integral ($\sim$3 eV), R_{C-C} the C–C bond length, and d_{CNT} is the tube diameter. The electronic DOS of a nanotube features van Hove singularities at each band minimum, associated with $1/\sqrt{(E - E_0)}$-like tails reflecting the free-electron character along the tube axis. Finally, in the π-conjugated molecules, the quantum confinement in all three dimensions gives rise to a set of discrete energy levels, as exemplified for C_{60} in Fig. 2C.

While all the carbon nanostructures in Fig. 1 have made their way into prototype or even close-to-application electronic devices, the inherent charge-transport characteristics and the factors that limit the charge-carrier mobility differ significantly among them. These differences directly mirror the electronic dimensionality and achievable dimensions of the respective π-systems. Graphene sheets can be easily prepared with micrometer sizes sufficient to connect electrodes accessible through standard lithography, thus opening the possibility to transport charges along graphene's extended π-system. By application of a control (gate) voltage, the charge carriers in graphene can be continuously tuned between electrons and holes in concentrations as high as 10^{13} cm^{-2}.[4] However, the zero band gap of graphene prevents effective current switching, which is essential for field-effect transistor (FET) operation. It is well documented that the carrier mobility in graphene is strongly influenced by the environment. Graphene sheets resting on a Si/SiO_2 substrate routinely reach mobilities of the order of 10 000 cm^2 V^{-1} s^{-1}.[4] In such devices, carrier scattering is likely to arise from charged surface impurities, which are typically present on Si/SiO_2 substrates with a density of $\sim 10^{12}$ cm^{-2}.[5] Scattering by trapped charges is expected to be especially effective close to the Dirac point, where the low carrier densities provide only weak screening. As an alternative scattering source, the formation of static ripples within the graphene sheet or the presence of graphene impurity states with an energy close to the charge neutrality (Dirac) point have been proposed.[6] Very recently, immense electron mobilities approaching 200 000 cm^2 V^{-1} s^{-1} have been detected at liquid-helium temperature in freely suspended graphene sheets (Fig. 3), indicative of near-ballistic transport over a micrometer length scale.[7,8] The suspended sheets, moreover, display a temperature-dependent minimum conductivity that approaches the theoretically predicted value of

Marko Burghard received his PhD in Physical Chemistry from the University of Tuebingen, Germany. In 1996, he joined the Max-Planck-Institute for Solid State Research in Stuttgart, where he started working on carbon nanotube-based electronics. His research focuses on the electrical and optical properties of chemically functionalized one- and two-dimensional nanostructures.

Hagen Klauk received a Diplom-Ingenieur degree in Electrical Engineering from Chemnitz University of Technology (Germany) in 1995, and a PhD degree in Electrical Engineering from the Pennsylvania State University (U.S.A.) in 1999. From 2000 to 2005 he was with the Polymer Electronics group at Infineon Technologies in Erlangen (Germany). In 2005 he joined the Max Planck Institute for Solid State Research in Stuttgart (Germany) to lead an Independent Junior Research Group in organic electronics.

Klaus Kern is Director and Scientific Member at the Max-Planck-Institute for Solid State Research in Stuttgart, Germany, Professor of Physics at the Ecole Polytechnique Fédérale de Lausanne (EPFL), Switzerland, and Honorary Professor at the University of Konstanz, Germany. His present research interests are in nanoscale science, self-ordering phenomena and in chemistry and physics of surfaces and interfaces. He holds a chemistry degree and PhD from the University of Bonn. After his doctoral studies he was staff scientist at the Research Center Jülich and visiting scientist at Bell Laboratories, Murray Hill before joining the Faculty of EPFL in 1991 and the Max-Planck-Society in 1998.

© 2009 WILEY-VCH Verlag GmbH & Co. KGaA, Weinheim

WILEY InterScience DISCOVER SOMETHING GREAT

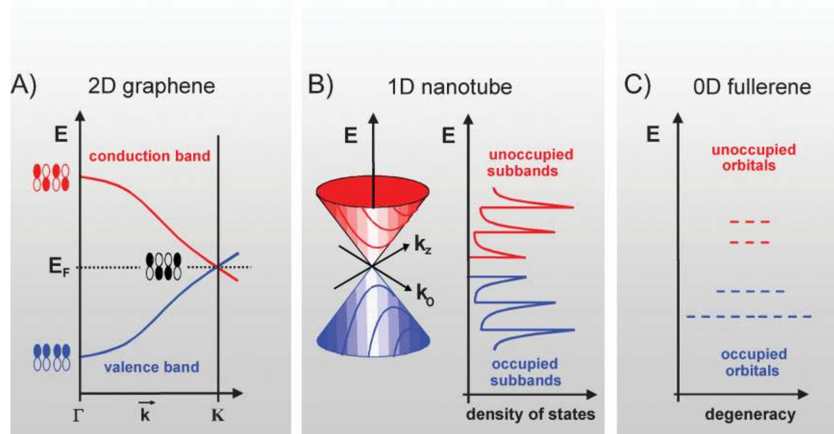

Figure 2. Schematic representation of A) a 1D section of the 2D band structure of graphene, B) the formation of 1D sub-bands in a carbon nanotube by restricting the wave vectors in circumferential direction and the resulting electronic DOS displaying van Hove singularities at the sub-band minima, and C) the set of discrete energy levels arising from the 3D confinement in C_{60}.

$4e^2 \cdot \pi h^{-1}$ at low temperatures (Fig. 3B). Notably, current-induced thermal annealing is a means to further remove surface contaminants.[8] With rising temperature, the carrier mobility is notably reduced, which has been attributed to acoustic phonon scattering[9,10] or extrinsic scattering by surface phonons at the underlying SiO_2 layer,[11] with the latter mechanism setting in at temperatures above 200 K.

In contrast to extended graphene sheets, the much smaller size of π-conjugated molecules renders it almost impossible to utilize the extended wave functions within the molecular plane for charge transport, unless considerable effort is spent, such as in specifically designed experiments on single molecules positioned inside nanogaps.[12] Therefore, technologically useful devices have to rely upon π-stacked molecule ensembles in the form of thin films, wherein the charge-transport direction is preferably perpendicular to the π-systems. Due to the fact that the molecular interactions in organic films are governed by relatively weak van der Waals forces and large intermolecular distances, the carrier-transport efficiency is expected to be substantially smaller than in covalently bound solids. In addition, the π-stack arrangement renders the charge transport highly sensitive with respect to structural defects, so that even moderate distortions, such as a single misplaced molecule, can significantly impede the charge transport through the stack. Indeed, the carrier field-effect mobilities of early organic transistors were quite small, on the order of 10^{-5}–0.01 $cm^2\ V^{-1}\ s^{-1}$.[13–16] Because of the small bandwidth of π-stacked organic semiconductor films, charge transport is typically described by carrier hopping. For organic semiconductors with mobilities of less than about 0.01 $cm^2\ V^{-1}\ s^{-1}$, the variable-range hopping (VRH) model has been developed.[17,18] However, in organic semiconductors with optimized thin-film morphology, mobilities up to $\sim$1 $cm^2\ V^{-1}\ s^{-1}$ are routinely achieved. To describe the electronic transport in organic films with such large mobilities (above about 0.1 $cm^2\ V^{-1}\ s^{-1}$), the multiple trapping and release (MTR) model has proven valuable,[19] although the existence of a true band-like transport in organic semiconductors is still under debate.

Similar to graphene, single-walled carbon nanotubes (SWCNTs) can be easily obtained with sufficient size to connect electrode pairs defined by standard lithography. Chemical vapor deposition (CVD) methods enable the routine growth of tens of micrometer long nanotubes from controlled surface sites by catalyst patterning on a substrate.[20] As a major difference to π-stacks of conjugated molecules, a CNT has a stronger capability to tolerate defects, because their impact is averaged out to some extent along the tube circumference, rendering them quite robust against elastic scattering.[21] High-quality SWCNTs exhibit at low temperatures ballistic transport over a micrometer length scale, as manifested by Fabry–Pérot-like interferences in the gate-dependence of the conductance.[22] At low applied bias, the charge transport is determined by inelastic scattering involving acoustic phonons, which imparts a 1/T-dependence of the carrier mobility on temperature in semi-conducting nanotubes.[23] Due to the weak electron-acoustic phonon coupling, semiconducting SWCNTs show extraordinary field-effect mobilities of up to several 10 000 $cm^2\ V^{-1}\ s^{-1}$.[24]

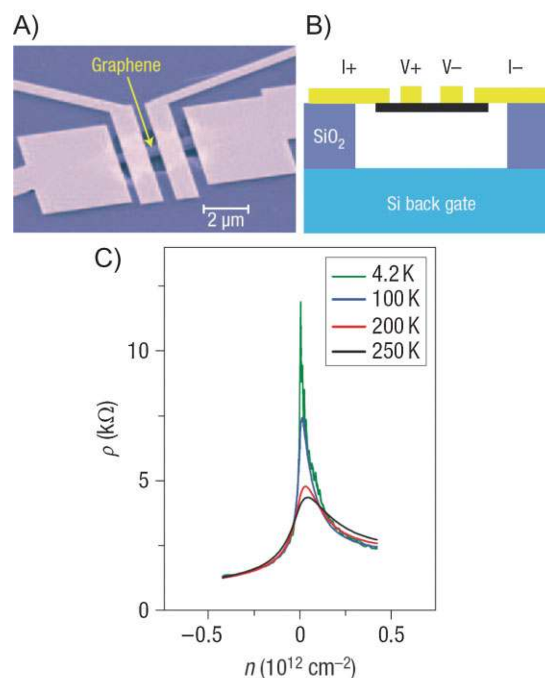

Figure 3. A) Electron microscopy image of a suspended graphene sheet in four-probe contact configuration implemented on a Si/SiO_2 substrate; B) schematic side view of the device. C) Plot of the resistivity of a suspended graphene sheet (0.5 µm length and 1.4 µm length), measured at four different temperatures, as a function of carrier density. Reproduced with permission from [7]. Copyright 2008 Nature Publishing Group.

© 2009 WILEY-VCH Verlag GmbH & Co. KGaA, Weinheim

At higher bias, the electrons gain sufficient energy to emit optical phonons. This type of scattering is considerably stronger compared to acoustic phonon scattering, and causes the current through an individual metallic or semiconducting nanotube to saturate at ~25 μA.[25] Akin to the π-conjugated molecules, the mobility of holes is larger than that of electrons in CNTs, which has been attributed to a thicker Schottky barrier for tunnel injection of electrons.

2. Carbon-Based Field-Effect Transistors

FETs are by far the most common electronic devices. Currently, about 10^{19} FETs are manufactured per year, most of them (~99%) on single-crystal silicon wafers as the building blocks of integrated circuits for microprocessors, solid-state memories, or mobile phones. The silicon serves as the substrate and as the semiconductor in which a channel of charge carriers (either negative electrons or positive holes) is accumulated by a transverse electric field from a conducting gate electrode. The gate electrode is usually a metal (or heavily doped polycrystalline silicon deposited by CVD) and is separated from the semiconductor by an insulating layer, the gate dielectric. Since, the carrier channel is located in close vicinity of the semiconductor/dielectric interface, the mobility of carriers in the channel is usually smaller than in the semiconductor bulk, due to interface scattering.[26] In the case of silicon, a gate dielectric with excellent bulk and interface quality is readily obtained by oxidizing the silicon surface at high temperature in dry oxygen. The thickness of the resulting SiO_2 layer can be scaled down to a few nanometers. This gate-dielectric scaling is necessary as the channel length of the transistor (the distance between the source contact, at which carriers are injected into the channel, and the drain contact, at which carriers are extracted) is further and further reduced. While the first microprocessors in the early 1970s had FETs with a channel length of 10 μm, 64-bit multicore processors currently in production utilize FETs with a channel length of 35 nm. In order to assure that the carrier density in the channel is controlled by the transverse gate field rather than by the lateral drain-source field, the thickness of the gate dielectric must also be aggressively reduced.

As a result of the continuous lateral and vertical scaling, state-of-the-art silicon FETs are nanoelectronic devices, but the miniaturization comes at a price. As the gate dielectric thickness is reduced below 2 nm, charge leakage due to quantum-mechanical tunneling increases to more than 1 A cm^{-2},[27] causing severe problems related to off-state current, power consumption, and heat dissipation. The leakage-current problem can be alleviated by replacing the thermally grown SiO_2 with a deposited metal oxide with larger permittivity (such as HfO_2), so that the same gate capacitance corresponds to a thicker dielectric (and hence smaller gate leakage). However, a deposited dielectric renders it more difficult to control the interface quality and scattering, so that the carrier mobilities are further reduced, to about 200 $cm^2\ V^{-1}\ s^{-1}$ for electrons and 40 $cm^2\ V^{-1}\ s^{-1}$ for holes,[28] and future scaling is likely to reduce the mobilities even further. Therefore, alternative semiconductors that are compatible with silicon technology platforms but provide higher carrier mobilities than silicon are of great interest, especially if they fit

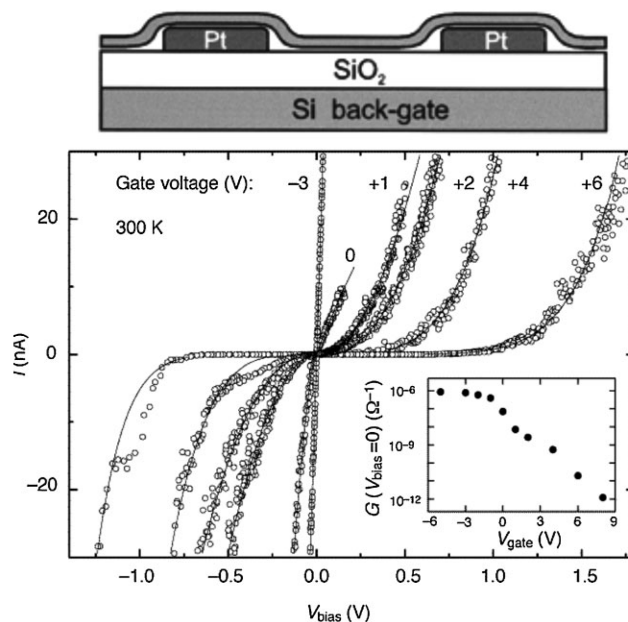

Figure 4. Schematic depiction of a FET comprising a single semiconducting SWCNT as conducting channel (top) and the gate-dependent current (*I*)-voltage (*V*) curves of the SWCNT-FET at room temperature (bottom). The inset shows the transfer characteristics of the device. Reproduced with permission from [29]. Copyright 1998 Nature Publishing Group.

naturally into a nanoscale FET architecture. An important milestone in this direction was the fabrication of the first carbon nanotube-based FET (Fig. 4) in 1998.[29] Since graphene and carbon nanotubes are characterized by very large mobilities and near-ballistic transport, these materials hold great promise for next-generation nanoelectronics.

While graphene and individual carbon nanotubes are of interest as an extension of silicon-based nanoelectronics, thin films of π-conjugated hydrocarbons offer the possibility of implementing electronic functionality in the form of FETs and integrated circuits on substrates other than silicon. For example, because all the functional materials required to build organic transistors can be deposited and patterned at or near room temperature, these devices can be manufactured on flexible, conformable, and even stretchable plastic substrates. This opens a range of new applications, such as roll-up displays, spherical focal-plane imaging arrays, and artificial skin (providing robots maneuvering in unstructured environments with a human-like sense of touch and temperature). These applications require that FETs and circuits be distributed on unconventional substrates over large areas, but they typically do not require high-frequency operation, so that the carrier mobilities of organic semiconductor films (~1 $cm^2\ V^{-1}\ s^{-1}$) are usually sufficient.

It is noteworthy that in addition to nanoscale FETs (based on graphene or carbon nanotubes) and flexible FETs (based on thin films of conjugated hydrocarbons), carbon-based transistors are also useful as chemical or biological sensors, because the environmental sensitivity of carbon-based molecules can be efficiently tailored by synthetic chemistry.[30] In the following sections, the focus will be laid on important recent advances in the development of FETs comprising the three different types of carbon nanostructures.

© 2009 WILEY-VCH Verlag GmbH & Co. KGaA, Weinheim
WILEY InterScience DISCOVER SOMETHING GREAT

3. FETs Comprising π-Conjugated Molecules

The concept of utilizing a deposited film of π-conjugated organic molecules as the active layer in a FET dates back more than 20 years.[13] The performance of the early organic transistors was limited by the fact that they utilized amorphous films characterized by poor orbital overlap. Over the years, a variety of strategies have been developed to improve molecular ordering, orbital coupling, and transport efficiency in deposited organic semiconductor films. This has resulted in carrier mobilities up to about 1 $cm^2 V^{-1} s^{-1}$, that is, similar to the mobilities observed in amorphous films of covalently bound semiconductors, such as hydrogenated amorphous silicon (a-Si:H).

The strategies developed to improve carrier transport in organic semiconductor films often involve the design of conjugated molecules with an enhanced potential for molecular self-organization. For example, by introducing alkyl chains at the end positions of planar conjugated oligomers, such as sexithiophene, the degree of long-range order in the films can be greatly enhanced compared with unmodified sexithiophene, resulting in significantly larger carrier mobilities.[31,32] In the case of semiconducting polymers, such as polythiophene, the potential for self-organization and hence orbital overlap and mobility can be substantially improved through the strategic substitution of alkyl chains,[33,34] and the inclusion of rotationally invariant, fused thiophene units along the polymer backbone.[35]

A second strategy to improve carrier transport in organic semiconductor films is tuning the process conditions in order to maximize the degree of molecular ordering realized during film growth. For vacuum-deposited organic semiconductors, film growth is efficiently controlled by adjusting the substrate temperature during deposition, with significant effects on the carrier mobility.[36–38] For solution-deposited semiconductors, film growth is controlled by the rate of solvent evaporation[39] and through thermally induced recrystallization.[35,40] In addition, the microstructure of both vacuum-deposited and solution-processed organic semiconductor films is greatly affected by the surface energy of the substrate surface, which can be conveniently controlled by chemical surface modifications.[41–43]

One of the most popular small-molecule semiconductors for organic transistors is the fused aromatic hydrocarbon pentacene. Pentacene has a strong tendency to crystallize, and upon vacuum deposition forms polycrystalline films with a high degree of molecular order. Figure 5 illustrates the thin-film morphology (imaged by atomic force microscopy)[44] and the relationship between the solid-state molecular arrangement (revealed by X-ray diffraction)[44] and the overlap of the delocalized molecular orbitals (computed from first principles)[45] for the thin-film polymorph of pentacene. The polycrystalline thin-film structure of pentacene evolves through the nucleation and growth of dendritic crystallites on the substrate surface, as shown in Figure 6.[46] The size of the crystallites and thus the density of grain boundaries is a function of the substrate properties and can be tuned by adjusting the growth conditions.

While the mobility of organic transistors has improved by five orders of magnitude since the first reports in the 1980s, the rate of improvement has recently slowed and other aspects of organic-transistor technology have been receiving increased attention. An example is the development of gate dielectrics that can be processed at temperatures sufficiently low to permit the use of flexible polymeric substrates, but which also provide a large capacitance that allows the transistors to be operated with usefully low supply voltages. One of the applications, for which low-voltage organic transistors are of interest, are flexible active-matrix organic light-emitting-diode (AM-OLED) displays.[47,48] State-of-the-art high-efficiency organic LEDs with doped injection layers produce a brightness of 1000 cd m^{-2} with supply voltages between 2.5 and 3 V (Fig. 7). In order to drive such OLEDs in a power-efficient AM display, the pixel drive transistors

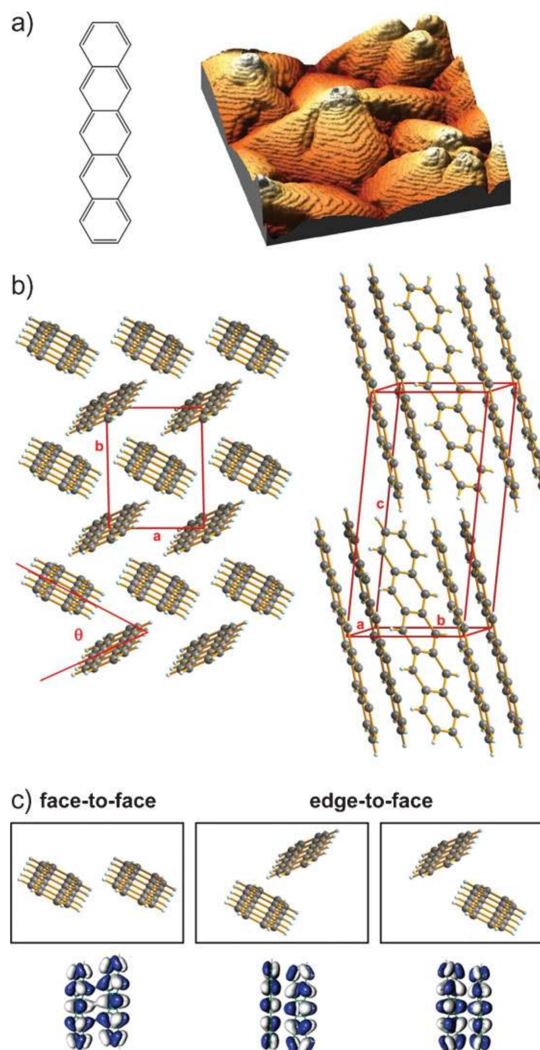

Figure 5. a) Morphology of a pentacene film grown by vacuum sublimation, imaged by atomic force microscopy. The image area is 2 μm × 2 μm. The height of the terraces corresponds to the thickness of a pentacene monolayer, with a layer spacing of 15.4 Å. Reproduced with permission from [44]. Copyright 2007 American Chemical Society. b) Crystal structure of the thin-film polymorph of pentacene, resolved by X-ray diffraction ($a = 5.96$ Å, $b = 7.60$ Å, $c = 15.61$ Å, $\alpha = 81.2^\circ$, $\beta = 86.6^\circ$, $\gamma = 89.8^\circ$, $\theta = 55$–60°). The *ab* plane is oriented parallel to the substrate surface. c) Overlapping of the HOMOs of next-neighbor molecules in the thin-film polymorph of pentacene. Reproduced with permission from [45]. Copyright 2005 American Chemical Society.

 © 2009 WILEY-VCH Verlag GmbH & Co. KGaA, Weinheim

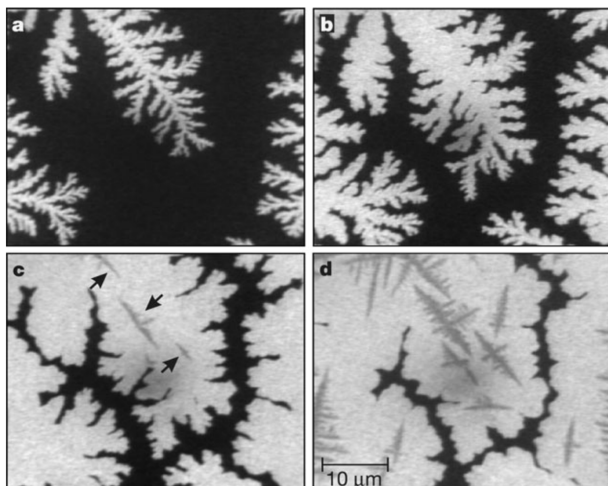

Figure 6. Evolution of the polycrystalline thin-film structure of pentacene deposited onto a hydrophobic, amorphous substrate. Reproduced with permission from [46]. Copyright 2001 Nature Publishing Group.

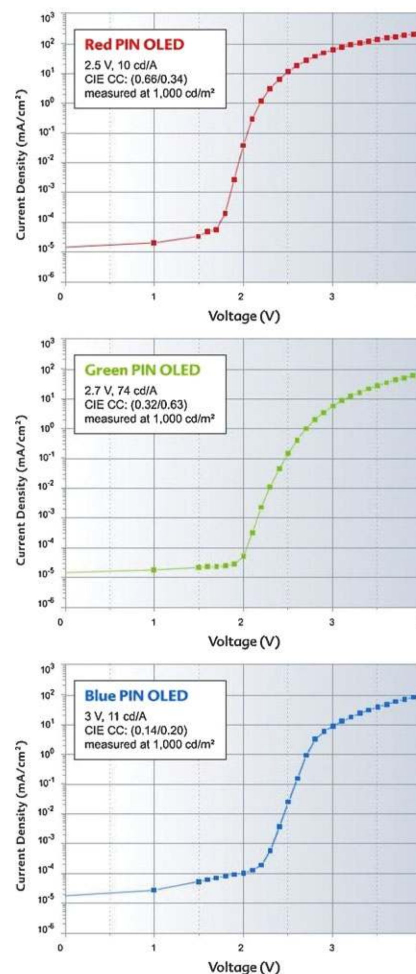

Figure 7. Current–voltage characteristics of state-of-the-art red, green, and blue small-molecule OLEDs with doped injection layers and low operating voltages (2.5–3 V, depending on emission color). Reproduced with permission from Novaled, Inc.

must be capable of operating with gate-source and drain-source voltages in the same range, that is, about 3 V.

A number of approaches toward low-temperature high-capacitance gate dielectrics for low-voltage organic transistors have been suggested. One is the use of inorganic metal oxide dielectrics with large permittivity, such as TiO_2,[49] Ta_2O_5,[48] ZrO_2,[50,51] and HfO_2.[52] These metal oxides provide capacitances ranging from 0.5 to 2 μF cm^{-2}, so that the transistors can be operated with voltages around 1–5 V. A second approach is the use of insulating polymers, such as polyimide, polystyrene, and polyvinylphenol, which are processed into films with a thickness of 10–20 nm. Although the permittivity of organic polymers is small (usually between 3 and 4), the small thickness of the spin-coated polymer films provides capacitances in the range of 0.2–0.3 μF cm^{-2}, and hence operating voltages of 2–3 V.[53,54] A third approach are solid polymer electrolytes or ion gels that form electric double layers and thus provide capacitances above 10 μF cm^{-2}, together with very large induced carrier densities and low operating voltages.[55–57] A fourth approach comprises self-assembled nanodielectrics based on well-defined aliphatic and polarizable molecular multilayers with a thickness of a few nanometers, providing a capacitance of 0.4 μF cm^{-2} and low-voltage transistor operation.[58]

Finally, low-temperature, high-capacitance gate dielectrics for organic transistors can be realized by combining a thin layer of an oxygen-plasma-grown metal oxide and a self-assembled monolayer (SAM) of an aliphatic phosphonic acid.[59–62] In this approach, the surface of the metal gate electrodes is oxidized at room temperature by an oxygen plasma. In the case of aluminum gate electrodes, this forms an AlO_x layer with a thickness of 3–4 nm, depending on the plasma power. This oxide layer alone is a poor dielectric characterized by substantial leakage currents. However, the plasma-grown oxide provides an excellent surface for the self-assembly of a molecular monolayer of an aliphatic phosphonic acid. This organic monolayer is obtained either by immersing the substrate in a 2-propanol solution of the phosphonic acid[59] or by transferring the monolayer from an elastomeric stamp,[60] followed by a brief anneal at a temperature of 70 °C. The SAM has a thickness of about 2.1 nm, giving a total AlO_x/SAM dielectric thickness of about 6 nm and a gate dielectric capacitance of ~0.7 μF cm^{-2}. Despite its small thickness and the low process temperature, the AlO_x/SAM dielectric provides acceptably small leakage currents of less than 10^{-5} A cm^{-2} at 3 V.

Figure 8 shows a photograph and the electrical characteristics of a pentacene transistor manufactured on a glass substrate with aluminum gate electrodes, a thin AlO_x/SAM gate dielectric, and gold source and drain contacts. Owing to the small thickness of the gate dielectric, the transistor can be operated with 3 V. The transistor has a carrier mobility of 0.6 cm^2 V^{-1} s^{-1}, an on/off current ratio of 10^7, and a sub-threshold swing of 100 mV per decade. The sub-threshold swing, defined as $S = \left(\mathrm{d}\,\log_{10} I/\mathrm{d}V_{\mathrm{gate}}\right)^{-1}$, is a measure of how effectively the gate switches the transistor current. Pentacene transistors with gold source and drain contacts display p-channel behavior, because the ionization potential of pentacene is similar to the work function of the gold contacts, so that the energy barrier for injecting positively charged carriers into the highest occupied

© 2009 WILEY-VCH Verlag GmbH & Co. KGaA, Weinheim
WILEY InterScience DISCOVER SOMETHING GREAT

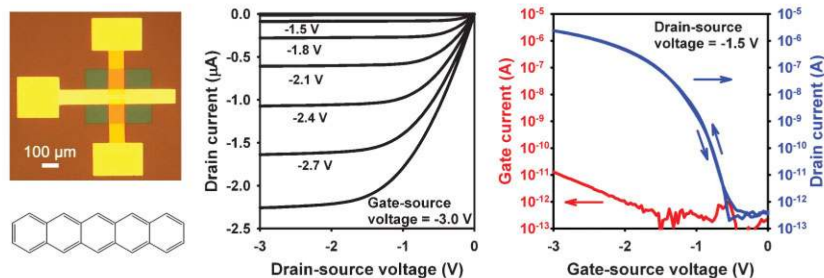

Figure 8. Photograph and electrical characteristics of a pentacene p-channel organic transistor manufactured on a glass substrate with aluminum gate electrodes, a thin AlO_x/SAM gate dielectric, and gold source and drain contacts. Owing to the small thickness of the gate dielectric, the transistor can be operated with 3 V. The transistor has a mobility of 0.6 $cm^2 V^{-1} s^{-1}$, an on/off current ratio of 10^7, and a sub-threshold swing of 100 mV per decade.

molecular orbital (HOMO) of pentacene is much smaller than the barrier for injecting negative carriers into the lowest unoccupied molecular orbital (LUMO).

In contrast to p-channel transistors, n-channel transistors require a material combination that provides good energy matching between the LUMO of the organic semiconductor and the work function of the source/drain metal. One possibility is to match the high-lying LUMO level of a conjugated hydrocarbon, such as pentacene, with a low-work-function metal, such as calcium. However, since low-work-function metals are quite reactive, and because electrons in the LUMO of organic semiconductors with a small electron affinity, such as pentacene, have poor stability in the presence of oxygen, such transistors cannot be operated in ambient air. An alternative is the synthesis of organic semiconductors with an electron affinity in the range of 4.2–4.6 eV, and the use of air-stable gold source and drain contacts. Such a large electron affinity is possible through the replacement of hydrogen with more electronegative substituents, such as fluorine or cyano groups. An example is hexadecafluorocopperphthalocyanine ($F_{16}CuPc$), which was first utilized in air-stable organic n-channel transistors in 1998.[63] Figure 9 shows the electrical characteristics of a low-voltage $F_{16}CuPc$ n-channel transistor on a glass substrate.

The possibility of manufacturing p-channel and n-channel organic transistors on the same substrate allows the realization of low-power organic complementary circuits, as shown in Figure 10. Compared with circuits based on a single carrier type (unipolar circuits), complementary circuits have a number of advantages, including smaller static-power consumption and sharper switching characteristics (larger output swing, higher small-signal gain, and greater noise margins).

The maximum switching speed of state-of-the-art organic complementary circuits is limited by the relatively low carrier mobility of the n-channel organic transistors (0.02 $cm^2 V^{-1} s^{-1}$ in the case of $F_{16}CuPc$). The small carrier mobility of $F_{16}CuPc$ is possibly related to poor molecular ordering in the phthalocyanine layer near the dielectric interface.[64] Organic complementary circuits with improved dynamic performance thus require an organic semiconductor with large electron affinity and good molecular ordering. Promising compounds toward this goal are perylene tetracarboxylic diimides (PTCDI) with electron-withdrawing substituents.[65] Figure 11 shows the electrical characteristics of an air-stable, low-voltage n-channel organic transistor based on a core-cyanated, fluoroalkyl-substituted PTCDI, with an electron mobility of 0.04 $cm^2 V^{-1} s^{-1}$. Even better performance may be expected from pentacene analogs with large electron affinity, such as azapentacene, which may combine the excellent molecular ordering of pentacene with an even larger electron affinity (and hence smaller energy barriers) than PTCDIs.[66]

4. Graphene-Based FETs

A major hurdle in the development of graphene field-effect devices is the lack of production methods that yield large amounts of well-defined graphene sheets. In fact, the often employed and already commercialized mechanical exfoliation of highly oriented pyrolytic graphite (HOPG),[67] developed in 2004,[4] is slow and yields only a few micrometer-sized flakes per square centimeter substrate area. Hence, increasing efforts are currently devoted toward alternative routes to graphene. Thus-far explored approaches rely upon the epitaxial growth or direct chemical synthesis of graphene, the liquid-phase exfoliation of graphite, as well as the conversion of graphene oxide (GO) to graphene. Epitaxial growth of graphene has been realized via vacuum graphitization of silicon carbide substrates,[68] and the catalytic decomposition of a gaseous precursor on metal substrates.[69] Regarding the chemical synthesis of graphene, besides the controlled bottom-up synthesis starting from smaller organic building blocks,[70] the gas-phase decomposition of a carbon source (for example, ethanol) inside a microwave plasma reactor is a promising method that affords few-layer graphene sheets of good structural quality.[71] Moreover, a solvothermal method involving the reductive decomposition of tetrachloromethane at $T = 100\,^{\circ}C$ has been reported to yield carbon nanosheets with a thickness between 3 and 8 nm.[72] Although these works represent first encouraging steps, it should be emphasized that significant improvements are still required in order to obtain extended, regular graphene monolayers. Efficient exfoliation of

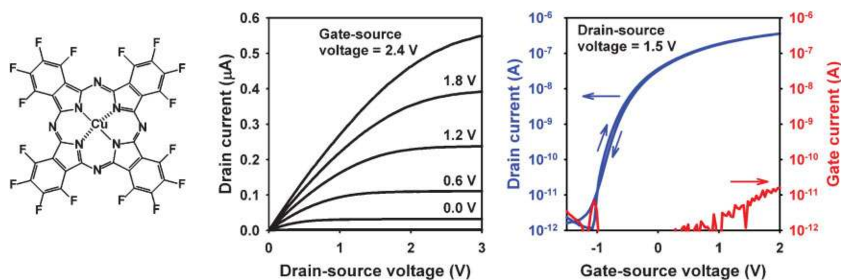

Figure 9. Electrical characteristics of a $F_{16}CuPc$ n-channel organic transistor manufactured on a glass substrate with aluminum gate electrodes, a thin AlO_x/SAM gate dielectric, and gold source and drain contacts. The transistor has a mobility of 0.02 $cm^2 V^{-1} s^{-1}$, an on/off current ratio of 10^5, and a sub-threshold swing of 160 mV per decade.

© 2009 WILEY-VCH Verlag GmbH & Co. KGaA, Weinheim

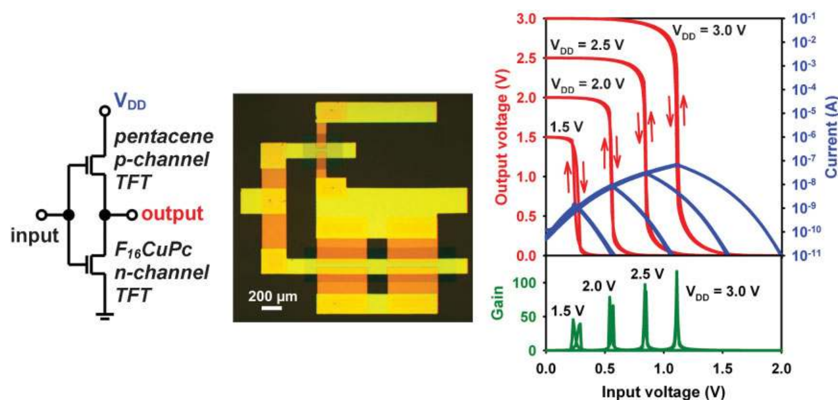

Figure 10. Photograph and static transfer characteristics of a low-voltage organic complementary inverter based on a pentacene p-channel transistor and a $F_{16}CuPc$ n-channel transistor.

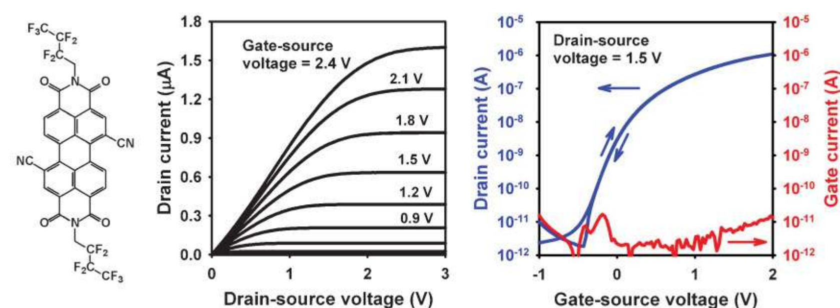

Figure 11. Electrical characteristics of a low-voltage PTCDI-FCN_2 n-channel organic transistor manufactured on a glass substrate with aluminum gate electrodes, a thin AlO_x/SAM gate dielectric, and gold source and drain contacts. The transistor has an electron mobility of 0.04 $cm^2 V^{-1} s^{-1}$, an on/off current ratio of 10^5, and a sub-threshold swing of 160 mV per decade. The chemical structure of PTCDI-FCN_2 is also shown.

graphite has very recently been accomplished through sonication of graphite within selected organic solvents, ensuring that the graphene–solvent interfacial-interaction energy matches that between the graphene layers.[73] While the resulting sheets with sizes of up to several micrometers appear to contain only a small amount of defects, their electrical characterization is still awaited. A higher yield of graphene can be obtained starting from expanded graphite that is accessible through intercalating graphite with a mixture of sulfuric acid and nitric acid, followed by rapidly heating the sample to 1000 °C, whereupon the formation of volatile gaseous species from the intercalants exfoliates the graphite into loosely associated graphene sheets.[74] Further processing by repeated intercalation, insertion of a tetrabutylammonium salt, and final sonication of the material within a surfactant solution yielded large amounts of suspended graphene monolayers.[75] The resulting graphene sheets constitute a suitable basis for the preparation of large transparent Langmuir–Blodgett (LB) films with good electrical conductivity. An overview of the wide variety of methods developed to obtain graphene through elimination of the oxygen-containing functional groups in GO is provided by Table 1. The common basis of these methods is the property of graphite oxide, usually prepared by Hummers method,[76] to readily exfoliate within an aqueous medium into single GO sheets (Fig. 12A). The subsequent chemical reduction of GO can be performed either within the aqueous colloid or after deposition of the GO sheets onto a substrate (Fig. 12B). In several cases, chemical functionalization in situ or prior to reduction has been employed to prevent agglomeration of the sheets, though appropriate reaction conditions lead to aqueous dispersions that are stable over weeks in ambient air without the need for stabilizing agents.[77,78]

The electrical conductivity of individual reduced GO monolayers has been found to be about three orders of magnitude smaller than that of mechanically exfoliated, solid-supported graphene.[79] The only-moderate electrical properties of GO-derived graphene result from a sizeable fraction of chemical defects like hydroxyl-, expoxide-, and carboxylic-groups that remain after the reduction, as corroborated by chemical analysis on bulk samples, which found a few percent of oxygenated functionalities.[80] Evidence for defective regions in reduced GO monolayers has been gained from Raman spectra, which display a pronounced D-band intensity comparable to that of the G-band. Moreover, signatures of defective regions with sizes of several nanometers are apparent in scanning tunneling microscopy (STM) images, as exemplified in Figure 12A (inset). In addition to oxides, point defects or even small holes are also likely to be introduced during graphite oxidation, although their presence and distribution remains to be evaluated, for which purpose transmission electron microscopy (TEM) could prove highly valuable.[81] The defects contained within the reduced GO sheets are held responsible for the prevalence of hopping instead of band-like electronic conduction in this material. It is plausible to assume that the hopping occurs through defective regions between the intact graphitic islands. As a potential advantage over pristine graphene, the defects contained in reduced GO may serve as anchors or nucleation sites for subsequent chemical functionalization. One possible modification is metal electrodeposition, which opens potential applications in chemical sensors.[82] Furthermore, it has been demonstrated that GO functionalized with a long-chain alkylamine can be processed into films, which after thermal deoxygenation at $T = 300$ °C show trap-free FET behavior, with charge-carrier mobilities of the order of 10 $cm^2 V^{-1} s^{-1}$ at room temperature.[83]

An essential prerequisite for graphene's application as an FET-channel material is to open its band gap. One possibility to achieve this task is to apply a perpendicular electric field to double-layer graphene. However, while prototype double-gate devices have already been demonstrated on this basis,[84] the magnitude of the induced gap (~10 meV) is still too small for room-temperature operation. Larger gaps have been attained through adsorption of the electron donor ammonia onto back-gated bilayers,[85] but such chemical doping is not

© 2009 WILEY-VCH Verlag GmbH & Co. KGaA, Weinheim

Table 1. Overview of chemical methods employed to convert GO to graphene

Deoxygenation agent/method	Means of stabilizing the dispersion	Type of medium or substrate	Reference
Hydrazine	Stable without stabilizer	Water	[77]
Hydroquinone	Precipitation	Water	[134]
(1) Borohydride (2) Hydrazine	Coupling of phenyl residues with SO_3^- groups	Water	[135]
Hydrazine	Absorption of 1-pyrenebutyrate	Water	[136]
Aqueous NaOH	Stable without stabilizer	Water	[78]
Hydrazine	Adsorption of negatively charged polyelectrolyte	Water	[80]
Hydrazine	Precipitation	Water	[137]
Hydrazine or hydrogen plasma	–	Si/SiO_2	[79,138]
Thermal annealing (up to 1100 °C)	–	Quartz	[139]
Hydrazine or thermal annealing (up to 1100 °C)	–	Quartz	[140]
Hydrazine or thermal annealing (>550 °C)	–	Quartz	[141]
Hydrazine	–	Si/SiO_2	[142]
Thermal annealing (1050 °C)	–	(Flakes)	[143]

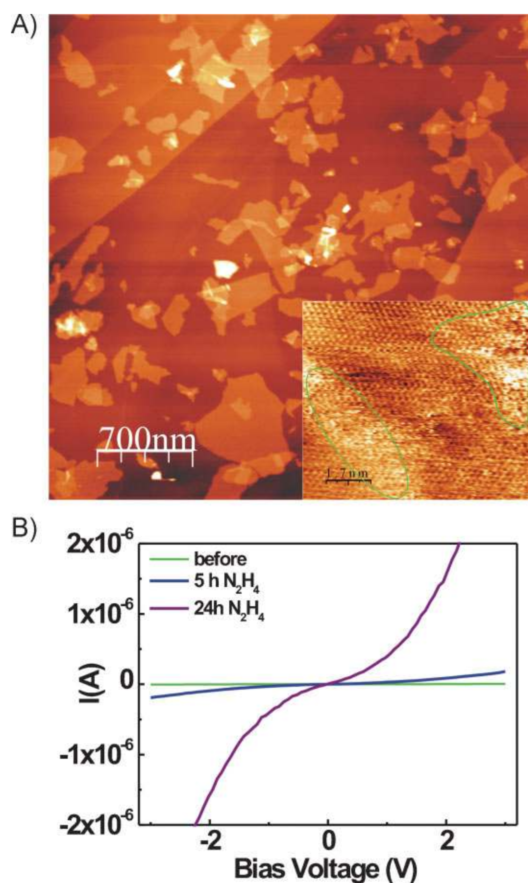

Figure 12. A) Atomic force microscopy image of GO sheets on a HOPG substrate. Cross-sectional profiles reveal that ~50% of the objects are monolayers. The inset shows an STM image recorded under ambient conditions from a chemically reduced GO monolayer. The bright regions encircled in green are attributed to the presence of remaining oxygenated functional groups and point defects, which are separating areas of intact hexagonal lattice structure. Reproduced with permission from [79]. Copyright 2007 American Chemical Society. B) Evolution of current (I)-voltage (V) characteristics upon chemical reduction of GO monolayers by exposure to hydrazine vapor.

compatible with common device technologies. An alternative approach to introduce a band gap in graphene is to constrict its lateral dimensions to produce quasi-1D graphene nanoribbons (GNRs). The quantization energy of GNRs can be considerably larger compared to conventional semiconductors due to graphene's linear energy dispersion and high Fermi velocity. According to theory, whether a GNR has a finite energy gap depends on its crystallographic orientation.[86] The confinement gap in a semiconducting GNR is expected to scale inversely with the ribbon width W according to $\Delta E = 2\pi\hbar v_F/3W$.[86,87] In the fabrication of the first GNR-based FETs, e-beam lithographic patterning followed by oxygen plasma etching was used, which afforded ribbon widths between 15 and 100 nm.[88,89] The conductance of the GNRs could be modulated by the applied gate potential over approximately one order of magnitude at room temperature, while at low temperature ($T = 4$ K), the ribbons displayed on/off ratios of up to 10^4. The energy gap, as determined from temperature-dependent conductance measurements, was found to be inversely proportional to the ribbon width, in accord with the theoretical prediction. For the narrowest ribbons ($W = 15$ nm), the energy gap reached a value of ~200 meV.[88] In contrast to the width dependence, no gap-size variation was observed between ribbons obtained by etching along different directions of the original graphene sheet. This finding reflects the dominant role of the edge structure compared to the ribbons' overall crystallographic orientation in determining their electrical behavior. The relevance of the edges is furthermore apparent from the observation that GNRs with widths below ~50 nm exhibited a trend toward increased resistivity, which is likely to originate from edge scattering.[89] Another fingerprint of edge effects is the fact that the experimentally observed 200 meV gap for a ribbon width of 15 nm is significantly larger than expected from the above relation.

A significant advancement has very recently been acheived by the development of a solution-based route to GNRs with smooth edges and widths down to a few nanometers (Fig. 13A). The procedure involves sonication of thermally exfoliated graphite obtained by the procedure described above in an organic solution of a π-conjugated organic polymer.[90] Electrical investigation of a range of these chemically derived GNRs with different widths revealed gate switching in all cases, testifying their all-

© 2009 WILEY-VCH Verlag GmbH & Co. KGaA, Weinheim

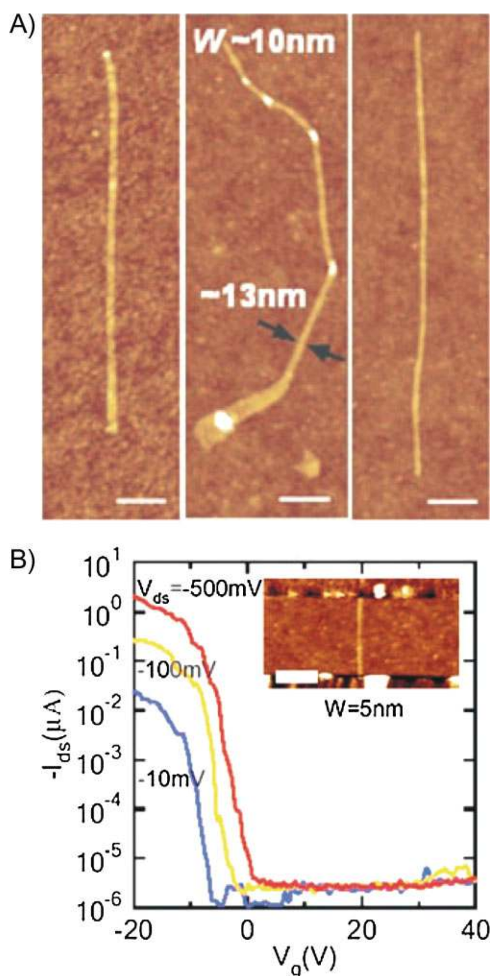

Figure 13. A) GNRs with a width of ~10 nm, obtained via sonication of thermally expanded graphite within a solution of a π-conjugated organic polymer. Scale bars: 100 nm. B) Drain-source current though a FET with a 5 nm wide GNR as conducting channel, measured at room temperature for three different drain-source voltages. Reproduced with permission from [90]. Copyright 2008 American Association for the Advancement of Science.

semiconductor nature, which constitutes a major advantage over SWCNTs (Fig. 13B). The energy gap of the narrowest ribbons ($W = 2$ nm) was estimated to be ~400 meV, a value in good agreement with theoretical predictions. The room-temperature performance of FETs incorporating ribbons less than 10 nm wide has been demonstrated to be comparable to SWCNT-FETs, as manifested by an on/off current ratio exceeding 10^6, a low sub-threshold swing of ~200 mV per decade, and an on-state current density as high as 2000 μA μm^{-1}.[91] Analogous to nanotube transistors, the GNR-FETs display unipolar p-type character, which has been ascribed to the high-work-function Pd electrodes producing close-to-Ohmic contact to the valence band. The room-temperature mobility of holes at low drain-source bias, reaching values close to 200 $cm^2\ V^{-1}\ s^{-1}$, has been interpreted to be limited mainly by elastic scattering at the ribbon edges. Interestingly, theoretical simulations suggest that the impact of the elastic scattering is reduced in the high-bias regime where optical phonon scattering gains relevance.[92] Of further interest is a novel approach toward GNRs, which relies upon controlled etching of graphene by metal catalyst particles. Etching of few-layer graphene along crystallographic axes has recently been demonstrated with the aid of thermally activated iron nanoparticles.[93]

The electrical characteristics of FETs comprising increasingly narrow GNRs reveal an increase in influence of contact barriers, a finding consistent with the assumption that the switching mechanism in these devices involves the modulation of Schottky barriers.[94,95] While contact barriers in GNR devices have so far only been studied by theory, recent scanning photocurrent microscopy (SPCM) measurements have provided useful information about the properties of metal contacts attached to larger graphene sheets (Fig. 14).[96] In this technique, the short-circuit photocurrent detected at zero drain-source bias is a measure of the local-electric-potential gradient. Evaluation of the gate-dependent short-circuit photocurrent at the contacts has revealed that gold as a high-work-function metal leads to local p-type doping of the sheet, whereas the low-work-function metal titanium imparts local n-type doping. The corresponding interfacial-potential steps have been determined to be −50 meV for gold and 30 meV for titanium at the Dirac point of the sheet. Notably, the contact doping leads to a p–p or p–n junction, depending on the polarity of carriers in the bulk of the sheet, which provides an explanation for the asymmetry in the electron and hole conduction observed in graphene devices.[97] This asymmetry has previously been ascribed to different scattering cross-sections off charged impurities for opposite carrier polarities.[98] Furthermore, gate-dependent SPCM images of graphene devices display a spatially inhomogeneous switching, with the transition from the p- to n-type conduction occurring earlier at the edge region than the sheet center. The charge accumulation at the sheet boundaries is at least in part attributable to the weaker local charge screening by the back gate separated by a 200 nm thick SiO_2 layer.[99] Further investigations are needed to clarify the extent to which edge defect states may additionally contribute to the observed behavior.

5. Carbon Nanotube-Based FETs

Although the operation mechanism of SWCNT-FETs is not yet fully understood, there is general consensus that they typically function as Schottky-barrier transistors rather than conventional bulk transistors. In the former type of transistor, the applied gate potential modulates not only the carrier density, but also the transmission through the Schottky barriers at the contacts, that is, both contact and channel resistance are affected by the gate.[100] The Schottky barrier for one carrier type can be minimized through a proper choice of contact metal, as has been first demonstrated by palladium contacts enabling nearly barrier-free access to the valence band of semiconducting tubes.[101] More recently, close-to-perfect contacts to the tube's conduction band have been accomplished using scandium, rendering both p- and n-type SWCNT-FETs available.[102] The influence of the Schottky barriers can be reduced by selectively doping the contact regions, as has been realized on the basis of strong chemical charge-transfer between the tube and adsorbed molecules.[103] In close correspondence to graphene devices, a convenient method to estimate the Schottky-barrier height in a semiconduct-

© 2009 WILEY-VCH Verlag GmbH & Co. KGaA, Weinheim
WILEY InterScience DISCOVER SOMETHING GREAT

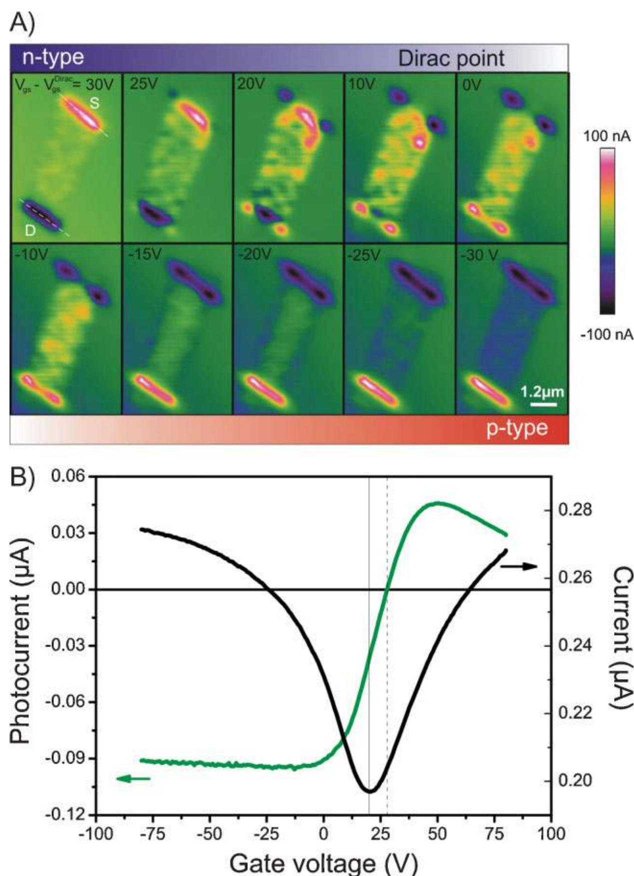

Figure 14. A) A series of SPCM images recorded at room temperature on a gold-contacted graphene monolayer as a function of back-gate voltage (at zero source-drain voltage). Upon transition from the n- to p-type regime, the photocurrent signs at the source and drain contact are inversed. B) For the same sheet, the local photocurrent at the center of the source electrode edge (green curve) and the dark source-drain current (black curve) is plotted versus gate voltage. The contact photoresponse can be used to determine the magnitude of the potential step at the gold/graphene interface and the local Fermi-level shift in the graphene. Reproduced with permission from [96]. Copyright 2008 Nature Publishing Group.

ing nanotube is SPCM performed under gate modulation.[104,105] It relies upon the fact that zero photocurrent is generated in the transistor off-state corresponding to the flat-band situation, whereas maximum photocurrent is observed at the switching threshold, that is, when the conduction-band edge aligns with the Fermi level of the contacts, for instance. In addition, SPCM has been used to determine the depletion layer width in the different device-operation regimes.[105]

In order to optimize the gate switching (minimize the sub-threshold swing S), the capacitive coupling of the gate electrode has to be enhanced. In the optimum case, the classical electrostatic capacitance C_g would become larger than the quantum capacitance C_q of the tube ($C_q = 10^{-16}$ F μm^{-1}),[106] and thus dominate the switching action.[107] Strong gate coupling has been implemented through a top gate separated from the nanotube by a layer a few nanometers thick of a high-permittivity (high-κ) dielectric, such as TiO_2 ($\kappa = 80$),[108] or HfO_2 ($\kappa = 25$).[109] The corresponding SWCNT-FETs display a sub-threshold swing close to the theoretically expected value of $S = 60$ mV per decade at room temperature, along with a large-scale transconductance of up to 5000 S m^{-1}. An alternative promising approach takes advantage of the excellent insulating capability of high-quality organic SAMs in combination with a thin, oxygen-plasma-grown oxide layer. SWCNT-FETs with a hybrid SiO_2/silane-based SAM gate insulator feature excellent device characteristics, including a low operation voltage of ~1 V and a sub-threshold swing of 60 mV per decade.[110] Another advantageous characteristic of these transistors is that the hysteresis is much smaller compared with devices in which the SWCNT is in direct contact with a hydrophilic SiO_2 surface.[111] Moreover, recent studies have shown that FETs with organic SAM-based gate dielectric do not only exhibit excellent device performance, but also high operation stability. This is exemplified in Figure 15 for an FET comprising an individual semiconducting nanotube with a lithographically patterned aluminum gate and a thin oxide/SAM gate insulator.[112] Such devices endure more than 10^4 on/off cycles without detectable loss of performance. In addition, they are stable for more than 300 days when stored in ambient air.

A long-standing problem in the fabrication of SWCNT-FETs is the lack of synthetic methods that yield exclusively semiconducting nanotubes, which has stimulated numerous attempts to either separate semiconducting tubes from the as-prepared material or to selectively eliminate the metallic tubes.[113] The separation approach has mainly relied upon noncovalent chemical functionalization by various types of polymers capable of selectively wrapping semiconducting SWCNTs, most prominently DNA[114] and polyfluorenes.[115] Moreover, self-sorting semiconducting-SWCNTs networks have been obtained by spin-coating nanotubes from solution onto appropriately surface-functionalized Si/SiO_2 substrates.[116] The principle of this method is based upon the selective binding of semiconducting tubes by the terminal amino groups of the silane layer on the silica.[117] Efficient chemical methods to eliminate the metallic tubes in nanotube ensembles include the coupling of benzene diazonium salts[118,119] and methane plasma etching.[120] In the latter process, the metallic nanotubes within an SWCNT film are preferentially modified, while semiconducting tubes with

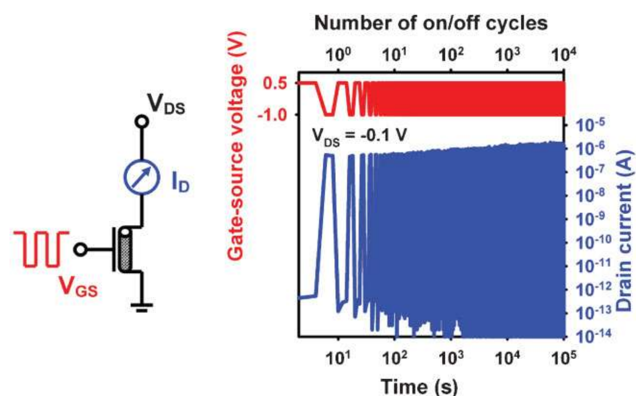

Figure 15. Gate cycling between the on and off states of an FET with an individual SWCNT on an SAM of an organic phosphonic acid attached as gate insulators onto the underlying aluminum electrode used as back gate. All measurements were performed under ambient conditions using a source-drain bias of −0.1 V.

© 2009 WILEY-VCH Verlag GmbH & Co. KGaA, Weinheim

diameters larger than 1.4 nm remain largely unaffected. The modified metallic tubes can then be permanently broken through thermal annealing. A reasonable explanation for the higher chemical reactivity of metallic tubes invokes their more-abundant delocalized electronic states favoring the formation of a transition state with electrophilic species.[121] Preferential destruction of metallic tubes has also been achieved through selective photo-oxidation using laser irradiation of appropriate wavelength.[122] More recently, it has been demonstrated that also long-arc Xe-lamp irradiation under ambient enables faster destruction of metallic over semiconducting tubes.[123] Another promising strategy involves substitution-doping of nanotubes. As a first step in this direction, the synthesis of SWCNTs co-doped with boron and nitrogen has recently been reported.[124] In agreement with theory, which predicts a band gap in the order of 0.5 eV for a 10% content of each boron and nitrogen, BCN-SWCNTs have been found to be purely semiconducting and well-suited as FET channels. FETs made of enriched semiconducting SWCNT ensembles easily reach large on/off ratios exceeding 10^5, which is sufficient for many applications.[114,116]

Significant progress has also been achieved in the development of FETs incorporating highly ordered SWCNT arrays produced via oriented CVD growth on quartz substrates, as illustrated in Figure 16A.[125] After transferring the arrays onto a polymer substrate and selective electrical breakdown of the metallic tubes, the devices display very good performance, including carrier mobilities approaching 1000 $cm^2\ V^{-1}\ s^{-1}$, scaled transconductances as high as 3000 $S\ m^{-1}$, and current outputs of up to 1 A. By combining p- and n-type FETs, with the latter obtained by chemical doping using a polymer rich in amino groups, logic gates such as CMOS inverters have also been realized. An extension of this work is the fabrication of integrated circuits comprising up to 100 random-network SWCNT-FETs on flexible plastic substrates (Fig. 16B).[126] Remarkably, even without enrichment of semiconducting tubes, the transistors display excellent performance, as reflected in sub-threshold swings as low as 140 mV per decade, mobilities of up to 80 $cm^2\ V^{-1}\ s^{-1}$, and operation voltages below 5 V. A key factor to achieve this has been to reduce the probability of metallic pathways through use of sufficiently narrow network stripes. Recent SPCM studies have provided electric-potential landscapes of SWCNT networks under different gating conditions, which could aid further optimization of the corresponding FET devices.[127]

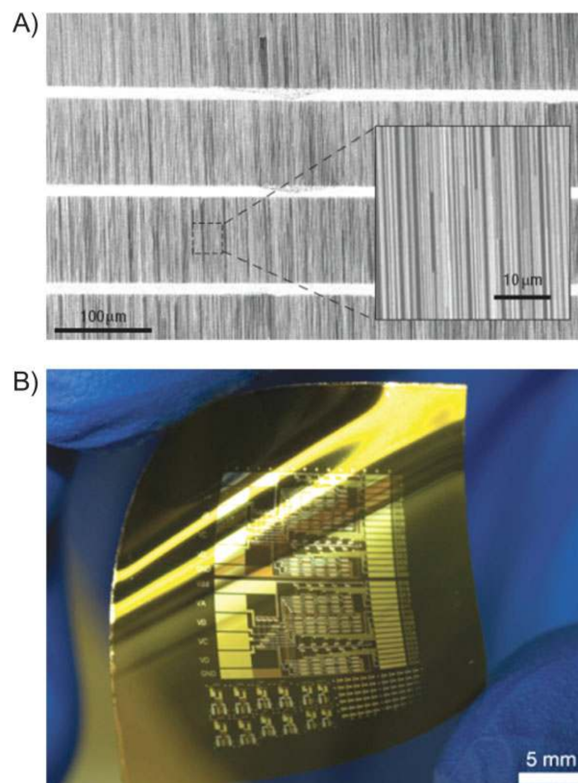

Figure 16. A) A pattern of laterally aligned SWCNTs grown by CVD on a quartz substrate. The densely packed arrays have been used as FET channels after electrical breaking of the contained metallic tubes. Reproduced with permission from [125]. Copyright 2007 Nature Publishing Group. B) Optical microscopy image of an integrated circuited consisting of several dozens of SWCNT-network transistors on a thin polyimide sheet. Reproduced with permission from [126]. Copyright 2008 Nature Publishing Group.

6. Conclusions

Among the different carbon nanostructures, carbon nanotubes are probably closest to real technological implementation into high-performance FET devices. This advance stems from the fact that (semiconducting) carbon nanotubes are the sole carbon nanostructure that combines several crucial features, namely the presence of a band gap, a big-enough size to enable electrical contacting with reasonable effort, as well as a low defect density and high stability. While still considerable effort is spent to drive SWCNT-based FETs to the ultimate performance limit, there is also an emerging trend of integrating the various nanostructures into novel, all-carbon device architectures. Theoretical studies have predicted that carbon-based conductive materials are advantageous over metal contacts for electrically contacting carbon nanostructures.[128] This is due to the possibility of direct bond formation between the carbon material and the nanostructure, with a character very similar to the internal bonding in the latter, thus ensuring a well-matched bonding network and a good continuity of electronic structure. As another advantage, the relatively small work-function difference among carbon nanostructures helps avoiding changes in the electrically addressed material due to contact doping. Moreover, in the particular case of carbon nanotubes, the tube diameter of 1–2 nm renders them close-to-ideal contacts for molecules.[129] Experimentally, first steps have already been undertaken toward integrating graphene and π-conjugated organics, as reflected by a very recent study using patterned graphene as bottom source and drain electrodes for efficient hole injection into a pentacene conduction channel.[130] Further to this, metallic SWCNTs have been utilized as electrical leads to contact pentacene nanocrystals.[131] Due to the favorable gate electrostatics of the sharp 1D electrode geometry, FETs obtained in this manner display orders of magnitude conductance modulation for channels of only several molecules in length. Another noteworthy development in this context is the use of carbon nanotubes as crystallization templates

© 2009 WILEY-VCH Verlag GmbH & Co. KGaA, Weinheim

WILEY InterScience DISCOVER SOMETHING GREAT

for the patterned growth of organic single crystals directly into device structures.[132] Besides integration approaches, also novel device concepts can be expected to become increasingly important in the future. One interesting example is electrical switching based upon the electric-field-induced motion of chains of carbon atoms in graphene. Pioneering experiments on graphene break junctions have shown that such switches can be extremely robust, which renders them interesting for information storage applications.[133]

Acknowledgements

M. B. and K. K. acknowledge funding by the Deutsche Forschungsgemeinschaft under the priority program 1121, and by the Landesstiftung Baden-Wuerttemberg through the Competence Network on Functional Nanostrucures. We thank B. Stuhlhofer at the Max Planck Institute for Solid State Research for expert technical assistance. This article is part of the Special Issue on Nanoionics.

Received: December 4, 2008
Revised: March 2, 2009
Published online: May 4, 2009

[1] H. Klauk, U. Zschieschang, R. T. Weitz, H. Meng, F. Sun, G. Nunes, D. E. Keys, C. R. Fincher, Z. Xiang, *Adv. Mater.* **2007**, *19*, 3882.
[2] A. M. van de Craats, J. M. Warman, A. Fechtenkötter, J. D. Brand, M. A. Harbison, K. Müllen, *Adv. Mater.* **1999**, *11*, 1469.
[3] H. Okamoto, N. Kawasaki, Y. Kaji, Y. Kubozono, A. Fujiwara, M. Yamaji, *J. Am. Chem. Soc.* **2008**, *130*, 10470.
[4] K. S. Novoselov, A. K. Geim, S. V. Morozov, D. Jiang, Y. Zhang, S. V. Dubonos, I. V. Grigorieva, A. A. Firsov, *Science* **2004**, *306*, 666.
[5] S. Adam, S. Das Sarma, *Solid State Commun.* **2008**, *146*, 356.
[6] M. I. Katsnelson, A. K. Geim, *Philos. Trans. R. Soc. Lond. A* **2008**, *366*, 195.
[7] X. Du, I. Skachko, A. Barker, E. Y. Andrei, *Nat. Nanotechnol.* **2008**, *3*, 491.
[8] K. I. Bolotin, K. J. Sikes, Z. Jiang, M. Klima, G. Fudenberg, J. Hone, P. Kim, H. L. Stormer, *Solid State Commun.* **2008**, *146*, 351.
[9] K. I. Bolotin, K. J. Sikes, J. Hone, H. L. Stormer, P. Kim, *Phys. Rev. Lett.* **2008**, *101*, 096802.
[10] A. Akturk, N. Goldsman, *J. Appl. Phys.* **2008**, *103*, 053702.
[11] J. H. Chen, C. Jang, S. D. Xiao, M. Ishigami, M. S. Fuhrer, *Nat. Nanotechnol.* **2008**, *3*, 206.
[12] H. Haick, D. Cahen, *Prog. Surf. Sci.* **2008**, *83*, 217.
[13] A. Tsumura, H. Koezuka, T. Ando, *Appl. Phys. Lett.* **1986**, *49*, 1210.
[14] A. Assadi, C. Svensson, M. Willander, O. Inganas, *Appl. Phys. Lett.* **1988**, *53*, 195.
[15] R. Madru, G. Guillaud, M. Al Sadoun, M. Maitrot, J. J. Andre, J. Simon, R. Even, *Chem. Phys. Lett.* **1988**, *145*, 343.
[16] G. Horowitz, D. Fichou, X. Peng, Z. Xu, F. Garnier, *Solid State Commun.* **1989**, *72*, 381.
[17] M. C. J. M. Vissenberg, M. Matters, *Phys. Rev. B* **1998**, *57*, 12964.
[18] M. Schwoerer, H. C. Wolf, *Organic Molecular Solids*, Wiley-VCH, Weinheim **2007**.
[19] G. Horowitz, R. Hajlaoui, P. Delannoy, *J. Phys. III* **1995**, *5*, 355.
[20] M. L. Terranova, V. Sessa, M. Rossi, *Chem. Vap. Deposition* **2006**, *12*, 315.
[21] C. T. White, T. N. Todorov, *Nature* **1998**, *393*, 240.
[22] J. Kong, E. Yenilmez, T. W. Tombler, W. Kim, H. J. Dai, R. B. Laughlin, L. Liu, C. S. Jayanthi, S. Y. Wu, *Phys. Rev. Lett.* **2001**, *87*, 106801.
[23] V. Perebeinos, J. Tersoff, P. Avouris, *Phys. Rev. Lett.* **2005**, *94*, 086802.
[24] T. Durkop, S. A. Getty, E. Cobas, M. S. Fuhrer, *Nano Lett.* **2004**, *4*, 35.
[25] Z. Yao, C. L. Kane, C. Dekker, *Phys. Rev. Lett.* **2000**, *84*, 2941.
[26] S. Takagi, A. Toriumi, M. Iwase, H. Tango, *IEEE Trans. Electr. Dev.* **1994**, *41*, 2357.
[27] S. H. Lo, D. A. Buchanan, Y. Taur, W. Wang, *IEEE Electr. Dev. Lett.* **1997**, *18*, 209.
[28] S.-C. Song, Z. Zhang, C. Huffman, J. H. Sim, S. H. Bae, P. D. Kirsch, P. Majhi, R. Choi, N. Moumen, B. H. Lee, *IEEE Trans. Electr. Dev.* **2006**, *53*, 979.
[29] S. J. Tans, A. R. M. Verschueren, C. Dekker, *Nature* **1998**, *393*, 49.
[30] K. Balasubramanian, M. Burghard, *Anal. Bioanal. Chem.* **2006**, *385*, 452.
[31] F. Garnier, A. Yassar, R. Hajlaoui, G. Horowitz, F. Deloffre, B. Servet, S. Ries, P. Alnot, *J. Am. Chem. Soc.* **1993**, *115*, 8716.
[32] M. Halik, H. Klauk, U. Zschieschang, G. Schmid, S. Ponomarenko, S. Kirchmeyer, W. Weber, *Adv. Mater.* **2003**, *15*, 917.
[33] Z. Bao, A. Dodabalapur, A. Lovinger, *Appl. Phys. Lett.* **1996**, *69*, 4108.
[34] B. S. Ong, Y. Wu, P. Liu, S. Gardner, *J. Am. Chem. Soc.* **2004**, *126*, 3378.
[35] I. McCulloch, M. Heeney, C. Bailey, K. Genevicius, I. MacDonald, M. Shkunov, D. Sparrowe, S. Tierney, R. Wagner, W. Zhang, M. L. Chabinyc, R. J. Kline, M. D. McGehee, M. F. Toney, *Nat. Mater.* **2006**, *5*, 328.
[36] B. Servet, G. Horowitz, S. Ries, O. Lagorsse, P. Alnot, A. Yassar, F. Deloffre, P. Srivastava, R. Hajlaoui, P. Lang, F. Garnier, *Chem. Mater.* **1994**, *6*, 1809.
[37] D. J. Gundlach, Y. Y. Lin, T. N. Jackson, S. F. Nelson, D. G. Schlom, *IEEE Electr. Dev. Lett.* **1997**, *18*, 87.
[38] R. T. Weitz, K. Amsharov, U. Zschieschang, E. Barrena Villas, D. K. Goswami, M. Burghard, H. Dosch, M. Jansen, K. Kern, H. Klauk, *J. Am. Chem. Soc.* **2008**, *130*, 4637.
[39] J. F. Chang, B. Sun, D. W. Breiby, M. M. Nielsen, T. I. Sölling, M. Giles, I. McCulloch, H. Sirringhaus, *Chem. Mater.* **2004**, *16*, 4772.
[40] K. C. Dickey, J. E. Anthony, Y. L. Loo, *Adv. Mater.* **2006**, *18*, 1721.
[41] Y. Y. Lin, D. J. Gundlach, S. F. Nelson, T. N. Jackson, *IEEE Electr. Dev. Lett.* **1997**, *18*, 606.
[42] H. Klauk, M. Halik, U. Zschieschang, G. Schmid, W. Radlik, W. Weber, *J. Appl. Phys.* **2002**, *92*, 5259.
[43] D. Knipp, R. A. Street, A. Völkel, J. Ho, *J. Appl. Phys.* **2003**, *93*, 347.
[44] S. Schiefer, M. Huth, A. Dobrinevski, B. Nickel, *J. Am. Chem. Soc.* **2007**, *129*, 10316.
[45] A. Troisi, G. Orlandi, *J. Phys. Chem. B* **2005**, *109*, 1849.
[46] F.-J. Meyer zu Heringdorf, M. C. Reuter, R. M. Tromp, *Nature* **2001**, *412*, 517.
[47] L. Zhou, A. Wanga, S. C. Wu, J. Sun, S. Park, T. N. Jackson, *Appl. Phys. Lett.* **2006**, *88*, 083502.
[48] M. Mizukami, N. Hirohata, T. Iseki, K. Ohtawara, T. Tada, S. Yagyu, T. Abe, T. Suzuki, Y. Fujisaki, Y. Inoue, S. Tokito, T. Kurita, *IEEE Electr. Dev. Lett.* **2006**, *27*, 249.
[49] L. A. Majewski, R. Schroeder, M. Grell, *Adv. Mater.* **2005**, *17*, 192.
[50] J. B. Koo, S. J. Yun, J. W. Lim, S. H. Kim, C. H. Ku, S. C. Lim, J. H. Lee, T. Zyung, *Appl. Phys. Lett.* **2006**, *89*, 033511.
[51] M. Zirkl, A. Haase, A. Fian, H. Schön, C. Sommer, G. Jakopic, G. Leising, B. Stadlober, I. Graz, N. Gaar, R. Schwödiauer, S. Bauer-Gogonea, S. Bauer, *Adv. Mater.* **2007**, *19*, 2241.
[52] J. Tardy, M. Erouel, A. L. Deman, A. Gagnaire, V. Teodorescu, M. G. Blanchin, B. Canut, A. Barau, M. Zaharescu, *Microelectron. Reliab.* **2007**, *47*, 372.
[53] M. H. Yoon, H. Yan, A. Facchetti, T. J. Marks, *J. Am. Chem. Soc.* **2005**, *127*, 10388.
[54] S. Y. Yang, S. H. Kim, K. Shin, H. Jeon, C. E. Park, *Appl. Phys. Lett.* **2006**, *88*, 173507.
[55] M. J. Panzer, C. D. Frisbie, *J. Am. Chem. Soc.* **2007**, *129*, 6599.
[56] J. H. Cho, J. Lee, Y. He, B. Kim, T. P. Lodge, C. D. Frisbie, *Adv. Mater.* **2008**, *92*, 686.
[57] J. H. Cho, J. Lee, Y. Xia, B. S. Kim, Y. He, M. J. Renn, T. P. Lodge, C. D. Frisbie, *Nat. Mater.* **2008**, *7*, 900.

© 2009 WILEY-VCH Verlag GmbH & Co. KGaA, Weinheim

[58] M. H. Yoon, A. Facchetti, T. J. Marks, *Proc. Natl. Acad. Sci.* **2005**, *102*, 4678.
[59] H. Klauk, U. Zschieschang, J. Pflaum, M. Halik, *Nature* **2007**, *445*, 745.
[60] U. Zschieschang, M. Halik, H. Klauk, *Langmuir* **2008**, *24*, 1665.
[61] T. Sekitani, Y. Noguchi, U. Zschieschang, H. Klauk, T. Someya, *Proc. Natl. Acad. Sci.* **2008**, *105*, 4976.
[62] P. H. Wöbkenberg, J. Ball, F. B. Kooistra, J. C. Hummelen, D. M. deLeeuw, D. D. C. Bradley, T. D. Anthopoulos, *Appl. Phys. Lett.* **2008**, *93*, 013303.
[63] Z. Bao, A. Lovinger, J. Brown, *J. Am. Chem. Soc.* **1998**, *120*, 207.
[64] D. G. de Oteyza, E. Barrena, S. Sellner, J. O. Osso, H. Dosch, *J. Phys. Chem. B* **2006**, *110*, 16618.
[65] B. A. Jones, M. J. Ahrens, M. H. Yoon, A. Facchetti, T. J. Marks, M. R. Wasielewski, *Angew. Chem. Int. Ed.* **2004**, *43*, 6363.
[66] M. Winkler, K. N. Houk, *J. Am. Chem. Soc.* **2007**, *129*, 1805.
[67] http://www.grapheneindustries.com (Accessed on April 14, 2009).
[68] C. Berger, Z. Song, X. Li, X. Wu, N. Brown, C. Naud, D. Mayou, T. Li, J. Hass, A. N. Marchenkov, A. H. Conrad, P. N. First, W. A. de Heer, *Science* **2006**, *312*, 1191.
[69] J. Coraux, A. T. N'Diave, C. Busse, T. Michely, *Nano Lett.* **2008**, *8*, 565.
[70] J. S. Wu, W. Pisual, K. Muellen, *Chem. Rev.* **2007**, *107*, 718.
[71] A. Dato, V. Radimilovic, Z. H. Lee, J. Phillips, M. Frenklach, *Nano Lett.* **2008**, *8*, 2012.
[72] Q. Kuang, S. Y. Xie, Z. Y. Jiang, X. H. Zhang, Z. X. Xie, R. B. Huang, L. S. Zheng, *Carbon* **2004**, *42*, 1737.
[73] Y. Hernandez, V. Nicolosi, M. Lotya, F. M. Blighe, Z. Y. Sun, S. De, I. T. McGovern, B. Holland, M. Byrne, Y. K. Gun'ko, J. J. Boland, P. Niraj, G. Duesberg, S. Krishnamurthy, R. Goodhue, J. Hutchinson, V. Scardaci, A. C. Ferrari, J. N. Coleman, *Nat. Nanotechnol.* **2008**, *3*, 563.
[74] D. Cho, S. Lee, G. M. Yang, H. Fukushima, L. T. Drzal, *Macromol. Mater. Eng.* **2005**, *290*, 179.
[75] X. L. Li, G. Y. Zhang, X. D. Bai, X. M. Sun, X. R. Wang, E. Wang, H. J. Dai, *Nat. Nanotechnol.* **2008**, *3*, 538.
[76] W. S. Hummers, R. E. Offeman, *J. Am. Chem. Soc.* **1958**, *80*, 1339.
[77] D. Li, M. B. Mueller, S. Gilje, R. B. Kaner, G. G. Wallace, *Nat. Nanotechnol.* **2008**, *3*, 101.
[78] X. Fan, W. Peng, Y. Li, X. Li, S. Wang, G. Zhang, F. Zhang, *Adv. Mater.* **2008**, *20*, 1.
[79] C. Gómez-Navarro, R. T. Weitz, A. M. Bittner, M. Scolari, A. Mews, M. Burghard, K. Kern, *Nano Lett.* **2007**, *7*, 3499.
[80] S. Stankovich, R. D. Piner, X. Q. Chen, N. Q. Wu, S. T. Nguyen, R. S. Ruoff, *J. Mater. Chem.* **2006**, *16*, 155.
[81] J. C. Meyer, C. O. Girit, M. F. Crommie, A. Zettl, *Nature* **2008**, *404*, 319.
[82] R. S. Sundaram, C. Gómez-Navarro, K. Balasubramanian, M. Burghard, K. Kern, *Adv. Mater.* **2008**, *20*, 3050.
[83] S. Wang, P.-J. Chia, L.-L. Chua, L.-H. Zhao, R.-Q. Png, S. Sivaramakrishnan, M. Zhou, R. G.-S. Goh, R. H. Friend, A. T.-S. Wee, P. K.-H. Ho, *Adv. Mater.* **2008**, *20*, 3440.
[84] J. B. Oostinga, H. B. Heersche, X. L. Liu, A. F. Morpurgo, L. M. K. Vandersypen, *Nat. Mater.* **2008**, *7*, 151.
[85] E. V. Castro, K. S. Novoselov, S. V. Mrozov, N. M. R. Peres, J. M. B. L. Dos Santos, J. Nilsson, F. Guinea, A. K. Geim, A. H. C. Neto, *Phys. Rev. Lett.* **2007**, *99*, 216802.
[86] Y. W. Son, M. L. Cohen, S. G. Louie, *Phys. Rev. Lett.* **2006**, *97*, 186801.
[87] V. Barone, O. Hod, G. E. Scuseria, *Nano Lett.* **2006**, *6*, 2748.
[88] M. Y. Han, B. Ozyilmaz, Y. B. Zhang, P. Kim, *Phys. Rev. Lett.* **2007**, *98*, 206805.
[89] Z. H. Chen, Y. M. Lin, M. J. Rooks, P. Avouris, *Phys. E* **2007**, *40*, 228.
[90] X. L. Li, X. R. Wang, L. Zhang, S. W. Lee, H. J. Dai, *Science* **2008**, *319*, 1229.
[91] X. R. Wang, Y. J. Ouyang, X. L. Li, H. L. Wang, J. Guo, H. J. Dai, *Phys. Rev. Lett.* **2008**, *100*, 206803.
[92] Y. J. Ouyang, X. R. Wang, H. J. Dai, J. Guo, *Appl. Phys. Lett.* **2008**, *92*, 243124.
[93] S. S. Datta, D. R. Strachan, S. M. Khamis, A. T. C. Johnson, *Nano Lett.* **2008**, *8*, 1912.
[94] G. C. Liang, N. Neophytou, M. S. Lundstrom, D. E. Nikonov, *Nano Lett.* **2008**, *8*, 1819.
[95] D. Jiménez, *Nanotechnology* **2008**, *19*, 345204.
[96] E. J. H. Lee, K. Balasubramanian, R. T. Weitz, M. Burghard, K. Kern, *Nat. Nanotechnol.* **2008**, *3*, 486.
[97] B. Huard, N. Stander, J. A. Sulpizio, D. Goldhaber-Gordon, *Phys. Rev. B* **2008**, *78*, 121402.
[98] J. H. Chen, C. Jang, S. Adam, M. S. Fuhrer, E. D. Williams, M. Ishigami, *Nat. Phys.* **2008**, *4*, 377.
[99] P. G. Sylvestrov, K. B. Efetov, *Phys. Rev. B* **2008**, *77*, 155436.
[100] S. Heinze, J. Tersoff, R. Martel, V. Derycke, J. Appenzeller, P. Avouris, *Phys. Rev. Lett.* **2002**, *89*, 106801.
[101] A. Javey, J. Guo, Q. Wang, M. Lundstrom, H. J. Dai, *Nature* **2003**, *424*, 654.
[102] Z. Y. Zhang, X. L. Liang, S. Wang, K. Yao, Y. F. Hu, Y. Z. Zhu, Q. Chen, W. W. Zhou, Y. Li, Y. G. Yao, J. Zhang, L. M. Peng, *Nano Lett.* **2007**, *7*, 3603.
[103] C. Klinke, J. Chen, A. Afzali, P. Avouris, *Nano Lett.* **2005**, *5*, 555.
[104] E. J. H. Lee, K. Balasubramanian, J. Dorfmueller, R. Vogelgesang, N. Fu, A. Mews, M. Burghard, K. Kern, *Small* **2007**, *3*, 2038.
[105] M. Freitag, J. C. Tsang, A. Bol, D. N. Yuan, J. Liu, P. Avouris, *Nano Lett.* **2007**, *7*, 2037.
[106] S. Ilani, L. A. K. Donev, M. Kindermann, P. L. McEuen, *Nat. Phys.* **2006**, *2*, 687.
[107] J. Appenzeller, J. Knoch, M. Radosavljevic, P. Avouris, *Phys. Rev. Lett.* **2004**, *92*, 226802.
[108] M. H. Yang, K. B. K. Teo, L. Gangloff, W. I. Milne, D. G. Hasko, Y. Robert, P. Legagneux, *Appl. Phys. Lett.* **2006**, *88*, 113507.
[109] Y. R. Lu, S. Bangsaruntip, X. R. Wang, L. Zhang, Y. Nishi, H. J. Dai, *J. Am. Chem. Soc.* **2006**, *128*, 3518.
[110] R. T. Weitz, U. Zschieschang, F. Effenberger, H. Klauk, M. Burghard, K. Kern, *Nano Lett.* **2007**, *7*, 22.
[111] J. B. Cui, R. Sordan, M. Burghard, K. Kern, *Appl. Phys. Lett.* **2002**, *81*, 3260.
[112] R. T. Weitz, U. Zschieschang, A. Forment-Aliaga, D. Kälblein, M. Burghard, K. Kern, H. Klauk, *Nano Lett.* **2009**, *9*, 1335.
[113] M. C. Hersam, *Nat. Nanotechnol.* **2008**, *3*, 387.
[114] L. Zhang, S. Zaric, X. M. Tu, X. R. Wang, W. Zhao, H. J. Dai, *J. Am. Chem. Soc.* **2008**, *130*, 2686.
[115] N. Izard, S. Kazaoui, K. Hata, T. Okazaki, T. Saito, D. Iijima, N. Minami, *Appl. Phys. Lett.* **2008**, *92*, 243112.
[116] M. C. LeMieux, M. Roberts, S. Barman, Y. W. Jin, J. M. Kim, Z. N. Bao, *Science* **2008**, *321*, 101.
[117] S. Auvray, V. Derycke, M. Goffman, A. Filoramo, O. Jost, J. P. Bourgoin, *Nano Lett.* **2005**, *5*, 451.
[118] M. S. Strano, C. A. Dyke, M. L. Usrey, P. W. Barone, M. J. Allen, H. W. Shan, C. Kittrell, R. H. Hauge, J. M. Tour, R. E. Smalley, *Science* **2003**, *301*, 1519.
[119] S. Toyoda, Y. Yamaguchi, M. Hiwatashi, Y. Tomonari, H. Murakami, N. Nakashima, *Chem. Asian J.* **2007**, *2*, 145.
[120] G. Y. Zhang, P. F. Qi, X. R. Wang, Y. R. Lu, X. L. Li, R. Tu, S. Bangsaruntip, D. Mann, L. Zhang, H. J. Dai, *Science* **2006**, *314*, 974.
[121] E. Joselevich, *Angew. Chem. Int. Ed.* **2004**, *43*, 2992.
[122] H. J. Huang, R. Maruyama, K. Noda, H. Kajiura, K. Kadono, *J. Phys. Chem. B* **2006**, *110*, 7316.
[123] Y. Y. Zhang, Y. Zhang, X. J. Xian, J. Zhang, Z. F. Liu, *J. Phys. Chem. C* **2008**, *112*, 3849.
[124] Z. Xu, W. Lu, W. Wang, C. Gu, K. Liu, X. Bai, E. Wang, H. J. Dai, *Adv. Mater.* **2008**, 3615.
[125] S. J. Kang, C. Kocabas, T. Ozel, M. Shim, N. Pimparkar, M. A. Alam, S. V. Rotkin, J. A. Rogers, *Nat. Nanotechnol.* **2007**, *2*, 230.
[126] Q. Cao, H. S. Kim, N. Pimparkar, J. P. Kulkarni, C. J. Wang, M. Shim, K. Roy, M. A. Alam, J. A. Rogers, *Nature* **2008**, *454*, 495.
[127] E. Lee, K. Balasubramanian, M. Burghard, K. Kern, see this special issue.

© 2009 WILEY-VCH Verlag GmbH & Co. KGaA, Weinheim

[128] Z. Qian, S. Hou, J. Ning, R. Li, Z. Shen, X. Zhao, Z. Xue, *J. Chem. Phys.* **2007**, *126*, 084705.
[129] Y.-R. Chen, L. Zhang, M. S. Hybertsen, *Phys. Rev. B* **2007**, *76*, 115408.
[130] C. A. Di, D. C. Wei, G. Yu, Y. Q. Liu, Y. L. Guo, D. B. Zhu, *Adv. Mater.* **2008**, *20*, 3289.
[131] P. Qi, A. Javey, M. Ronaldi, Q. Wang, E. Yenilmez, H. Dai, *J. Am. Chem. Soc.* **2004**, *126*, 11774.
[132] S. Liu, A. L. Briseno, S. C. B. Mannsfeld, W. You, J. Locklin, H. W. Lee, Y. Xia, Z. Bao, *Adv. Funct. Mater.* **2007**, *17*, 2891.
[133] B. Standley, W. Bao, H. Zhang, J. Bruck, C. N. Lau, M. Bockrath, *Nano Lett.* **2008**, *8*, 3345.
[134] G. X. Wang, J. Yang, J. Park, X. L. Gou, B. Wang, H. Liu, J. Yao, *J. Phys. Chem. C* **2008**, *112*, 8192.
[135] Y. Si, E. T. Samulski, *Nano Lett.* **2008**, *8*, 1679.
[136] Y. X. Xu, H. Bai, G. W. Lu, C. Li, G. Q. Shi, *J. Am. Chem. Soc.* **2008**, *18*, 5856.
[137] S. Stankovich, D. A. Dikin, R. D. Piner, K. A. Kohlhaas, A. Kleinhammes, Y. Jia, Y. Wu, S. T. Nguyen, R. S. Ruoff, *Carbon* **2007**, *45*, 1558.
[138] S. Gilje, S. Han, M. Wang, K. L. Wang, R. B. Kaner, *Nano Lett.* **2007**, *7*, 3394.
[139] X. Wang, L. J. Zhi, K. Müllen, *Nano Lett.* **2008**, *8*, 323.
[140] H. A. Becerril, J. Mao, Z. Liu, R. M. Stoltenberg, Z. Bao, Y. Chen, *ACS Nano* **2008**, *2*, 463.
[141] G. Eda, G. Fanchini, M. Chhowalla, *Nat. Nanotechnol.* **2008**, *3*, 270.
[142] J. T. Robinson, F. K. Perkins, E. S. Snow, Z. Q. Wei, P. E. Sheehan, *Nano Lett.* **2008**, *8*, 3137.
[143] H. C. Schniepp, J. L. Li, M. J. McAllister, H. Sai, M. Herrera-Alonso, D. H. Adamson, R. K. Prud'homme, R. Car, D. A. Saville, I. A. Aksay, *J. Phys. Chem. B* **2006**, *110*, 8535.

 WILEY InterScience® DISCOVER SOMETHING GREAT

© 2009 WILEY-VCH Verlag GmbH & Co. KGaA, Weinheim